EPJ Web of Conferences **95**, 04075 (2015)
DOI: 10.1051/epjconf/20159504075

Identified charged hadron production in pp, p–Pb and Pb–Pb collisions at LHC energies with ALICE

Giacomo Volpe[1,a], on behalf of the ALICE Collaboration

[1] *CERN, CH1211 Geneva 23, Switzerland*

Abstract. The ALICE detector is dedicated to the study of strongly interacting matter in the extremely high temperature and energy density conditions reached in relativistic heavy-ions collisions at the LHC. ALICE has unique particle identification (PID) capabilities among the LHC experiments thanks to the use of the combination of different PID techniques, i.e. energy loss and time of flight measurements, Cherenkov and transition radiation detection, calorimetry and topological ID.
The latest results on charged pions, kaons and (anti)protons transverse momentum (p_{T}) spectra, ratios and integrated yields, measured in pp collisions at $\sqrt{s}$ = 7 TeV and $\sqrt{s}$ = 2.76 TeV, Pb–Pb collisions at $\sqrt{s_{\mathrm{NN}}}$ = 2.76 TeV and p-Pb collisions at $\sqrt{s_{\mathrm{NN}}}$ = 5.02 TeV, will be presented. The nuclear modification factors as a function of p_{T}, for Pb–Pb and p–Pb interactions, will be shown. The results from different colliding systems will be compared. These will also be compared with calculations from hydrodynamical and statistical hadronization models.

1 Introduction

ALICE [1] is designed to study the physics of strongly interacting matter under the extremely high temperature and energy density conditions reached in the relativistic heavy-ion collisions, to investigate the properties of the quark-gluon plasma (QGP). pp collisions, as high energy QCD reference, and proton-nucleus collisions, as control experiment to test the initial/cold nuclear matter state effects, are also studied. The transverse momentum, p_{T}, distributions of identified charged hadrons contain relevant information about the collective expansion of the system ($p_{\mathrm{T}} < 2$ GeV/c), the presence of new hadronization mechanisms like quark recombination (2 GeV/$c < p_{\mathrm{T}} < 8$ GeV/c) [2] and, at higher p_{T}, the possible modification of the fragmentation due to the medium [3, 4]. ALICE has reported the transverse momentum spectra, as a function of the Pb–Pb collision centrality and p–Pb event multiplicity of $\pi^{\pm}$, $\mathrm{K}^{\pm}$ and $\mathrm{p}(\bar{\mathrm{p}})$ from low (hundreds of MeV/c) [5, 6] to high (15–20 GeV/c) [7] p_{T}. In this work complementary measurements on identified charged hadrons production measured in different colliding systems and in a wide momentum range are presented.

2 Analysis method

The results presented here are obtained from a sample of the data collected during the LHC Pb–Pb run at $\sqrt{s_{\mathrm{NN}}}$ = 2.76 TeV in 2010 and 2011, the p–Pb run at $\sqrt{s_{\mathrm{NN}}}$ = 5.02 TeV in the beginning of 2013

[a] e-mail: giacomo.volpe@cern.ch

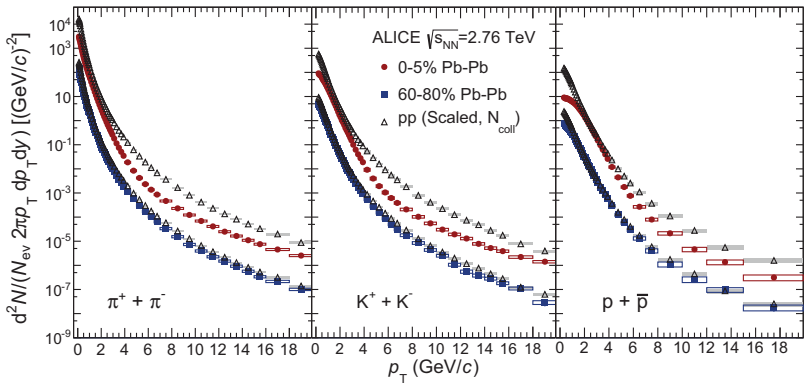

Figure 1. (Color online) Solid markers show the invariant p_{T}-differential yields of identified particles in central (circles) and peripheral (squares) Pb−Pb collisions [7]. Open points show the pp reference yields scaled by the average number of binary collisions for 0-5% (circles) and 60-80% (squares) [15]. The statistical and systematic uncertainties are shown as vertical error bars and boxes, respectively.

and the pp run at $\sqrt{s} = 2.76$ TeV in 2011. The event and track selection criteria are described in [5–8]. We present results for primary particles, defined as all particles produced in the collision, including decay products, but excluding weak decays of strange particles. The Pb−Pb collision centrality is determined from the measured amplitude in the VZERO counters [9], two arrays of 32 scintillator tiles each covering the full azimuth within $2.8 < \eta_{\mathrm{lab}} < 5.1$ (VZERO-A) and $-3.7 < \eta_{\mathrm{lab}} < -1.7$ (VZERO-C), which is related to the number of participating nucleons through simulations based on a Glauber model [10]. For p−Pb collisions, the nucleon-nucleon center-of-mass system has a rapidity of $y_{\mathrm{NN}} = -0.465$ in the direction of the proton beam due to the asymmetric beam energies. Due to the weak correlation between collision geometry and multiplicity, particle production is studied in seven multiplicity event classes instead of centrality. This selection is based on cuts on the total charge deposited in the VZERO-A (Pb beam direction) detector [6]. Charged hadron identification in the low p_{T} region in the central barrel is performed with the Inner Tracking System (ITS), the Time Projection Chamber (TPC) [11] and Time-Of-Flight (TOF) [12] detectors. The drift and strip layers of the ITS provide a measurement of the specific energy loss with a resolution of about 10%. The TPC provides particle identification at low momenta via specific energy loss $\mathrm{d}E/\mathrm{d}x$ in the fill gas with a resolution of about 6.5% in the 0−5% most central Pb−Pb collisions. The separation power achieved in p-Pb collisions is closer to that in pp collisions ($\sigma_{\mathrm{d}E/\mathrm{d}x} \approx 5.2\%$) [13]. The TOF array allows identification at higher p_{T} measuring the particle speed with the time-of-flight technique. The total time resolution is about 80 ps for events in the multiplicity classes from 0% to 80%. In more peripheral Pb−Pb or p−Pb collisions, where multiplicities are similar to pp, it decreases to about 120 ps due to a worse resolution in the start-time (collision-time) determination [13]. In pp and Pb−Pb collisions the PID is further improved at intermediate p_{T} (1.5 GeV/c < p_{T} < 6 GeV/c) using the High Momentum PID (HMPID) Cherenkov detector [14]. HMPID enables 3σ separation up to 3 GeV/c for π/K and up to 5 GeV/c for K/p. Identification at higher p_{T} is done using the specific energy loss, $\mathrm{d}E/\mathrm{d}x$, measured in the fill gas of the TPC in the relativistic rise region.

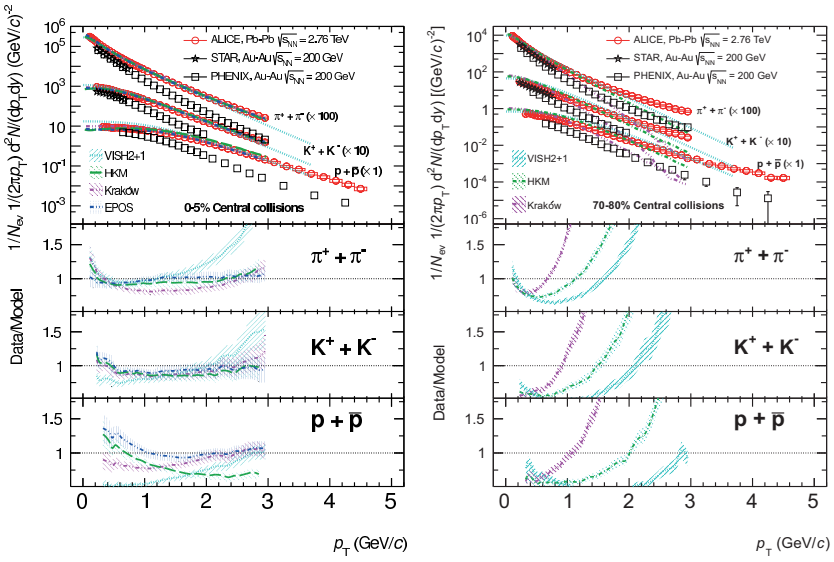

Figure 2. (Color online) Transverse momentum spectra of charged pions, kaons and (anti)protons measured in central (left) and peripheral (right) Pb–Pb collisions at $\sqrt{s_{NN}}$ = 2.76 TeV [5]. The results are compared with measurements at RHIC and with hydrodynamical models.

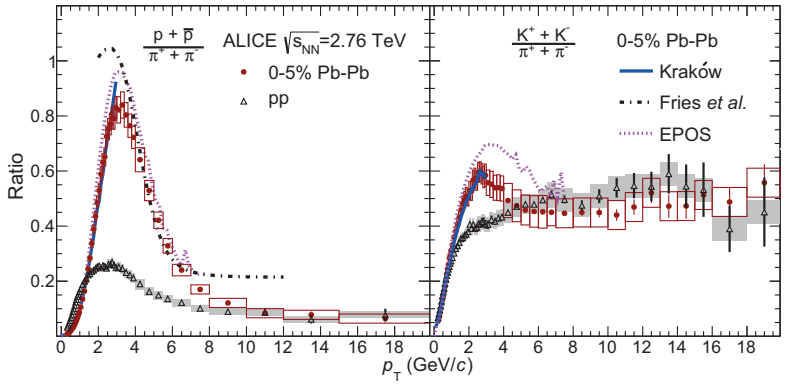

Figure 3. (Color online) Particle ratios as a function of p_T measured in pp and in the most central, 0-5%, Pb–Pb collisions [7]. Statistical and systematic uncertainties are displayed as vertical error bars and boxes, respectively.

3 Results

3.1 Spectra and ratios

Fig. 1 [7] shows the invariant p_T-differential yields measured in Pb–Pb collisions compared with those in pp collisions scaled by the number of binary collisions, N_{coll} [15]. For central Pb–Pb collisions, the spectra show a reduction in the production of high-p_T particles with respect to the reference which

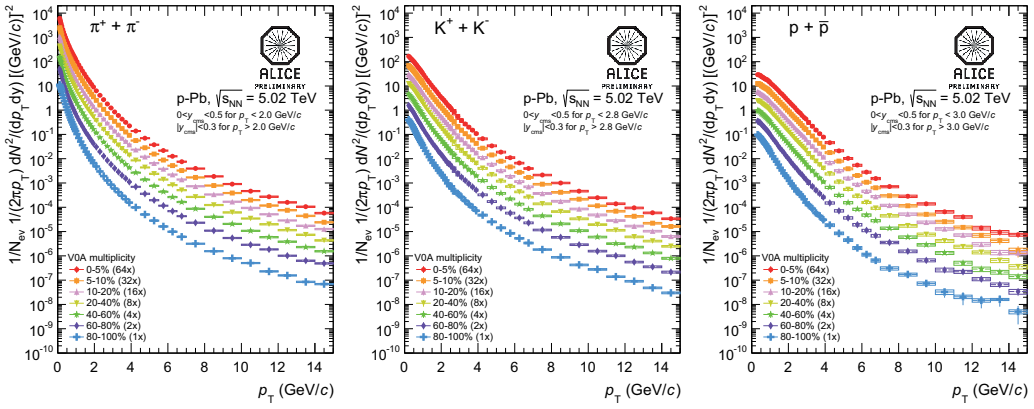

Figure 4. (Color online.) Invariant p_{T}-differential yields of $\pi^{\pm}$, $\mathrm{K}^{\pm}$, and $\mathrm{p}(\bar{\mathrm{p}})$ measured in p−Pb collisions in different VZERO-A multiplicity classes.

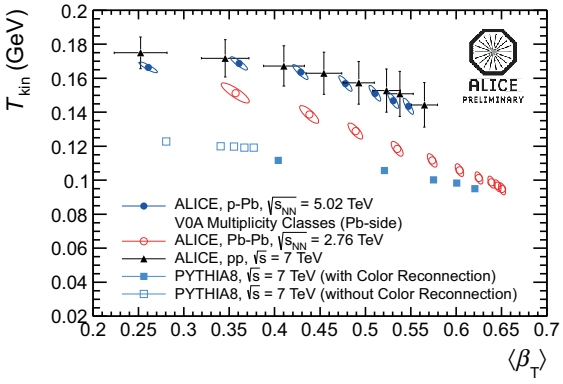

Figure 5. (Color online.) Results of blast-wave fits, compared with Pb−Pb data and MC simulations from PYTHIA8 with and without color reconnection. Charged-particle multiplicity increases from left to right. Uncertainties on the fits parameters are shown as correlation ellipses.

is characteristic of jet quenching. For peripheral Pb−Pb collisions the shapes of the invariant yields are similar to those observed in pp collisions. In Pb−Pb collisions, p_{T} spectra have been compared with predictions from hydrodynamic models. In Fig. 2 (left) [5] models give a fair description of the data for central collisions. In the region $p_{\mathrm{T}} < 3$ GeV/c (Kraków [16]), $p_{\mathrm{T}} < 1.5$ GeV/c (HKM [17]), and $p_{\mathrm{T}} < 3$ GeV/c (EPOS [18], with the exception of protons), the models describe the experimental data within $\approx 20\%$, supporting a hydrodynamic interpretation of the p_{T} spectra in central collisions at the LHC. A general feature of these models is that, going to more peripheral events, the theoretical curves deviate from the data at high p_{T} (Fig. 2 right [5]). This is similar to what is observed in the comparison with the blast-wave fits and shows the limits of the hydrodynamical models. Fig. 3 shows the proton-to-pion and kaon-to-pion ratios as a function of p_{T} in central Pb−Pb collisions. The ratio

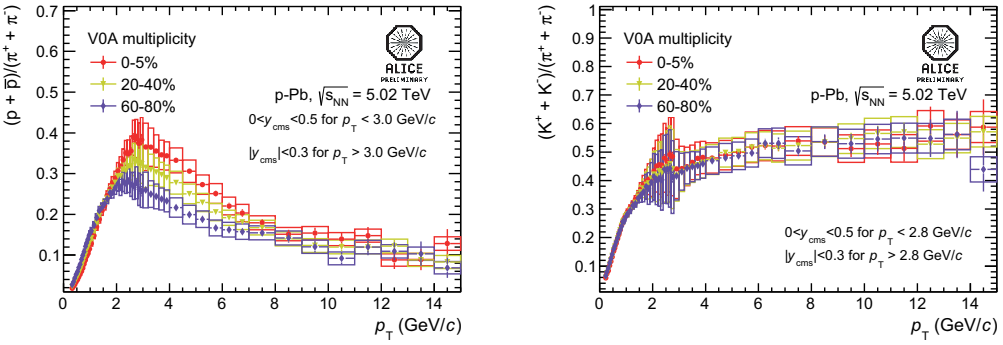

Figure 6. (Color online) Proton-to-pion ratio (left) and kaon-to-pion ratio (right) as a function of p_T measured in p−Pb collisions at $\sqrt{s} = 5.02$ TeV.

$(p + \bar{p})/(\pi^+ + \pi^-)$ reaches ≈ 0.83 at the maximum around 3 GeV/c and then decreases with increasing p_T. This value is approximately 20% above the peak values measured at RHIC [19, 20]. Predictions where recombination only occurs for soft thermal radially flowing partons are, as shown in the figure, more consistent with the data [21]. Surprisingly, in central Pb−Pb collisions the $(K^+ + K^-)/(\pi^+ + \pi^-)$ ratio also exhibits a bump at $p_T \approx 3$ GeV/c. This has not been observed at RHIC but is also observed in the soft coalescence model [21]. The Kraków hydrodynamical model captures the rise of both ratios quantitatively well. For higher p_T (>10 GeV/c) both particle ratios behave like those in pp, suggesting that fragmentation dominates the hadron production. In Fig. 4 the transverse momentum spectra of $\pi^{\pm}$, $K^{\pm}$ and $p(\bar{p})$ are shown for the seven VZERO-A multiplicity event classes measured in p-Pb collisions. For p_T below 2 GeV/c the spectra become harder as the multiplicity increases and the effect is stronger for heavier particles. This feature is reminiscent of what is observed in heavy-ion collisions where it is attributed to the hydrodynamical evolution of the medium, and in fact the p_T spectra measured in high multiplicity p−Pb collisions are better described by models which incorporate hydrodynamics [6]. To study the evolution of the spectral shapes with multiplicity the blast-wave analysis has been performed and the results are shown in Fig. 5. It is possible to compare the results from different colliding systems (pp, p−Pb and Pb−Pb) using a small set of parameters, which, in heavy-ion collisions are typically connected with the kinetic freeze-out temperature (T_{kin}) and the radial flow ($\langle\beta_T\rangle$). Figure 5 shows that a qualitatively similar behaviour is obtained for the three systems, even in PYTHIA 8 events simulated with Color Reconnection [22]. The proton-to-pion and kaon-to-pion ratios have been also evaluated for p−Pb collisions. The results are presented in Fig. 6 for three multiplicity intervals. For p_T below (above) ≈ 2 GeV/c the $(p + \bar{p})/(\pi^+ + \pi^-)$ ratios exhibit a depletion (enhancement) from low to high multiplicity. The highest (lowest) multiplicity interval gives ratios which reaches maxima at $p_T \approx 3$ GeV/c amounting to ≈ 0.4 (≈ 0.28). Above 3 GeV/c, the ratios start to decrease down to ≈ 0.1 at $p_T \approx 10$ GeV/c, which according to [8] corresponds to the value measured for vacuum fragmentation (pp collisions). The $(K^+ + K^-)/(\pi^+ + \pi^-)$ ratio saturates at 0.5 for high p_T as in Pb−Pb collisions and it does not show strong multiplicity dependence.

3.2 Integrated yields and thermal models

The data are fitted and extrapolated outside the measured p_T range and the integrated production yields dN/dy are obtained using the measured data points and the extrapolation. The production

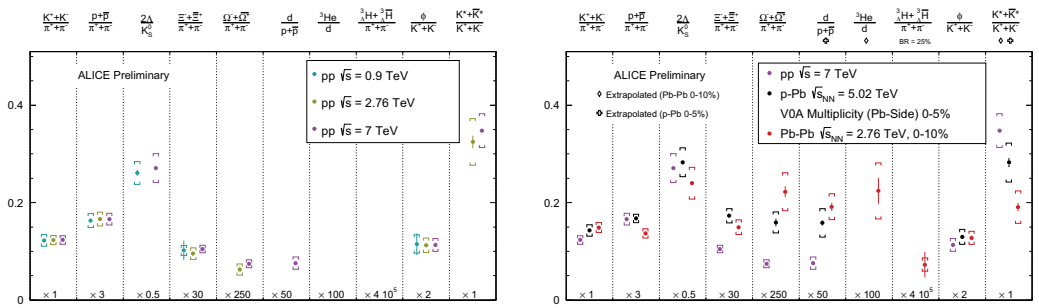

Figure 7. (Color online) (left) Particle ratios in pp collisions for different $\sqrt{s}$ (^{3}He and $^3_\Lambda$H are not yet measured in pp collisions at the LHC). (Right) Particle ratios in pp, p−Pb, and Pb−Pb collisions at LHC energies.

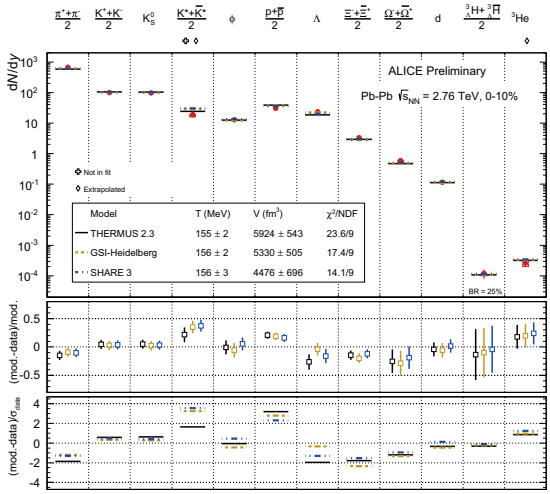

Figure 8. (Color online) Thermal fit of particle yields in 0-10% central Pb−Pb collisions.

yields of several particle species have been measured in pp collisions at $\sqrt{s}$ = 0.9, 2.76, and 7 TeV, no significant changes in particle ratios within uncertainties are observed, as shown in Fig. 7 (left). In Fig. 7 (right) particle ratios from different colliding systems are compared. The particle ratios evolve as a function of the system size, passing from small (pp), intermediate (p−Pb) to large (Pb−Pb) collisions system. Strangeness and deuteron enhancement is observed as well as K* and baryon suppression. The p_{T}-integrated yields and ratios can be interpreted in terms of statistical (thermal) models. ALICE data is compared with the calculations of three statistical hadronization models (Fig. 8), THERMUS 2.3 [23], GSI-Heidelberg [24] and SHARE 3 [25]. Temperature and fireball volume are fitted to the data. The respective best fit yields very similar parameters and reveals a possible anomalous suppression of proton yields in central Pb-Pb collisions at the LHC.

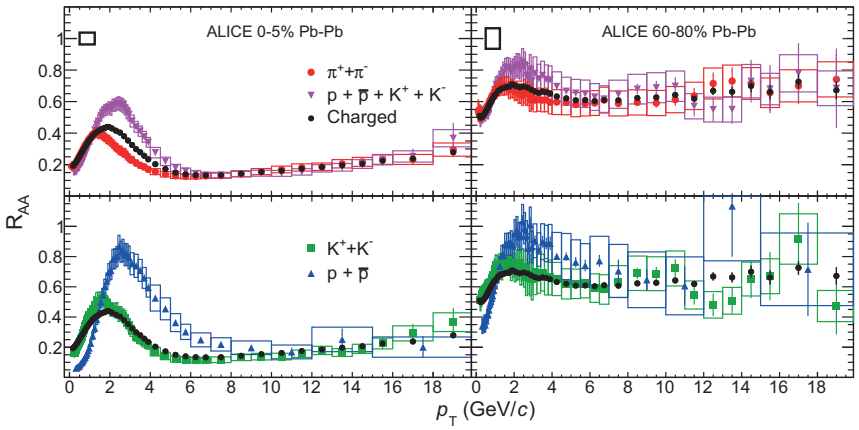

Figure 9. (Color online) The nuclear modification factor $R_{\rm AA}$ as a function of $p_{\rm T}$ for different particle species [7]. Results for 0−5% (left) and 60−80% (right) Pb−Pb collision centralities are shown. Statistical and systematic uncertainties are plotted as vertical error bars and boxes around the points, respectively. The total normalization uncertainty (pp and Pb−Pb) is indicated by the black boxes in the top panels [26].

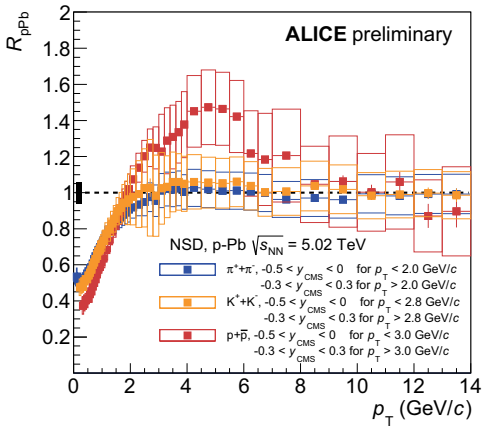

Figure 10. (Color online) $R_{\rm pA}$ of pions, kaons, and (anti)protons in NSD p−Pb at $\sqrt{s}$ = 5.02 TeV.

3.3 Nuclear modification factor

The nuclear modification factor $R_{\rm AA}$ defined as the ratio of the Pb−Pb spectra to the $N_{\rm coll}$ scaled pp spectra is shown as a function of $p_{\rm T}$ in Fig. 9. $R_{\rm AA}$ for the sum of kaons and protons is shown as it allows the most precise quantitative comparison with the $R_{\rm AA}$ of pions. Protons appear to be less suppressed than kaons and pions for $p_{\rm T} < 10$ GeV/c, in agreement with the particle ratios shown in Fig. 3. At larger $p_{\rm T}$ (>10 GeV/c) all particle species are equally suppressed. Despite the strong energy loss observed in the most central heavy-ion collisions, the particle composition and ratios at high $p_{\rm T}$ are similar to those in vacuum. In Fig. 10 the nuclear modification factor of pions, kaons and (anti)protons in NSD p−Pb collisions is shown. For pions and kaons it is flat over the measured $p_{\rm T}$ range. Protons exhibit a peak at intermediate $p_{\rm T}$ showing a mass ordering in the Cronin region [27].

4 Conclusions

Pion, kaon and (anti)proton production measured by ALICE in pp, p−Pb and Pb−Pb collisions have been presented. Central Pb−Pb collisions spectral shapes and ratios are fairly well described by hydrodynamical models. The nuclear modification factor in Pb−Pb collisions for $p_{\mathrm{T}} > 10$ GeV/c does not depend on particle specie: chemical composition of leading particles from jets in the medium is similar to that of vacuum jets. Thermal (statistical) models describes particle production well in Pb−Pb collisions. p−Pb collisions show similarity at high multiplicity with Pb−Pb collisions; spectra are well described by hydrodynamical models, hinting to an indication of final state effects due to hydrodynamics. However, other mechanisms, like Multiple Partons Interaction plus Color Reconnection, can also produce flow-like patterns without the presence of any medium [22].

References

[1] K. Aamodt, et al., J. Instrum. **3**, S08002 (2008).
[2] R. J. Fries, V. Greco, P. Sorensen, Ann. Rev. Nucl. Part. Sci. **58**, 177-205 (2008).
[3] S.Sapeta, U.A.Wiedemann, Eur. Phys. J C **55**, 293-302 (2008).
[4] R. Bellwied, C. Markert, Phys. Lett. B **691**, 208-213 (2010).
[5] B. Abelev, et al., Phys. Rev. C **88**, 044910 (2013).
[6] B. B. Abelev, et al., Phys. Lett. B **728**, 25-38 (2014).
[7] B. Abelev, et al., Phys. Lett. B **736**, 196-207 (2014).
[8] B. Abelev, et al., Phys. Rev. Lett. **109**, 252301 (2012).
[9] E. Abbas, et al., J. Instrum. **8**, P10016 (2013).
[10] B. Abelev, et al., Phys. Rev. C **88**, 044909 (2013).
[11] J. Alme, Y. Andres, H. Appelshauser, et al., Nucl. Instrum. Methods Phys. Res., Sect. A, Accel. Spectrom. Detect. Assoc. Equip. **622** 316-367 (2010).
[12] A. Akindinov, A. Alici, et al., Eur. Phys. J. Plus **128** 44 (2014).
[13] Int. J. Mod. Phys. A **29** 1430044 (2014).
[14] CERN/LHCC 98-19, ALICE TDR 1.
[15] B. Abelev, et al., Phys. Rev. C **88**, 044909 (2013).
[16] P. Bozek, I.Wyskiel-Piekarska, Phys. Rev. C **85**, 064915 (2012).
[17] I. Karpenko, Y. Sinyukov, K. Werner, Phys. Rev. C **87**, 024914 (2013).
[18] K. Werner, et al., Phys. Rev. C **85**, 064907 (2012).
[19] A. Adare, et al., Phys. Rev. C **88**, 024906 (2013).
[20] B. Abelev, et al., Phys. Rev. Lett. **97**, 152301 (2006).
[21] R.J. Fries, B. Müller, C. Nonaka, S.A. Bass, Phys. Rev. C **68**, 044902 (2003).
[22] A. Ortiz Velasquez, et al., Phys. Rev. Lett. **111** (4) 042001 (2013) .
[23] J. Cleymans et al., Phys. Rev. C **74**, 034903 (2006).
[24] A. Andronic et al., Nucl. Phys. A **772**, 167 (2006).
[25] J. Rafelski et al., arXiv:1310.5108 [hep-ph].
[26] B. Abelev, et al., Phys. Lett. B **720** 52-62 (2013).
[27] P.B. Straub et al ., Phys. Rev. Lett. **68**, 452 (1992).